SLAC-PUB-12998
November 2007

Extracting longitudinal shower development information from crystal calorimetry plus tracking

D.N. Brown [a], J. Ilic [b], G.B. Mohanty [b]
[a] *Lawrence Berkeley National Laboratory, Berkeley, California 94720, USA*
[b] *Department of Physics, University of Warwick, Coventry CV4 7AL, United Kingdom*

Abstract

We propose a novel approach to derive longitudinal shower development information from a longitudinally unsegmented calorimeter such as the *BABAR* electromagnetic calorimeter by utilizing tracking information in conjunction with that of calorimetry. We show that using this information as part of an electron identification algorithm results in a significant reduction in the pion misidentification probability for low momentum particles. We also demonstrate how this information provides general charged particle separation at low momentum, particularly between pions and muons.

Key words: Particle Identification, Longitudinal Shower Depth, Electromagnetic Calorimetry, Tracking
PACS: 29.40.Gx, 29.40.Vj, 07.05.Kf

1. Introduction

Precision electromagnetic calorimetry plays a key role in many present-day High Energy Physics experiments, as well as future experiments envisioned at the LHC [1] and the ILC [2]. It is particularly important for an efficient detection of photons and a clean identification of electrons, two important ingredients of many physics studies. Inorganic scintillating crystals, such as NaI(Tl) and CsI(Tl), are often used to construct electromagnetic calorimeters when a precise measurement of the energy is required [3]. Crystal calorimeters can be finely segmented in the dimension transverse to the shower development without sacrificing energy resolution, thus providing a good measurement of the lateral shower development. However, engineering and energy resolution considerations prevent finely segmenting crystal calorimeters along the direction of shower development, thus they cannot directly provide information on the longitudinal shower development. Both lateral and longitudinal shower development information are useful in charged particle identification (PID) algorithms, particularly in electron identification. Because crystal calorimeters cannot provide direct longitudinal shower development information, they lose an important cross-check on particle identification.

In this paper, we present a novel technique in which longitudinal shower development information is indirectly extracted from a longitudinally unsegmented crystal calorimeter in conjunction with a precise tracking system. This algorithm was developed for use with *BABAR* [4], but it can be applied to any detector which combines crystal calorimetry and precision tracking. We demonstrate that using the derived longitudinal shower development information as part of an electron identification algorithm improves the electron *vs.* pion discrimination.

Email addresses: Dave_Brown@lbl.gov (D.N. Brown), J.Ilic@warwick.ac.uk (J. Ilic), G.B.Mohanty@warwick.ac.uk (G.B. Mohanty).

Submitted to Nuclear Instrumentation and Methods (NIM) A

Work supported in part by US Department of Energy contract DE-AC02-76SF00515

We also show that this information can be used to improve the separation of the five most common stable charged particles (e, μ, π, K and p), owing to the different longitudinal shower development in a crystal calorimeter of these different particle types. Furthermore, we verify that the energy dependence of the indirect electron longitudinal shower information behaves as expected from models based on detailed electromagnetic shower depth measurements made directly in segmented calorimeters.

2. The *BABAR* Detector

The *BABAR* detector consists of a tracking system surrounded by a dedicated particle identification device, a crystal calorimeter, and an array of flux return iron plates instrumented with muon detectors. A detailed description of the *BABAR* detector can be found in Ref. [4], here we briefly describe those systems important for the algorithm described in this paper.

The *BABAR* tracking system is composed of a silicon vertex tracker (SVT) comprising five layers of double-sided detectors and a 40-layer central drift chamber (DCH). Operating in a 1.5 T solenoidal magnetic field, it provides a transverse momentum (p_T) resolution

$$\frac{\sigma_{p_T}}{p_T} = (0.13 \pm 0.01)\% \cdot p_T \oplus (0.45 \pm 0.03)\% \qquad (1)$$

for detecting charged particles, where p_T and σ_{p_T} are measured in GeV/c. Both the DCH and the SVT measure the specific ionization (dE/dx) of charged particles which pass through them. The dE/dx resolution from the DCH varies as a function of track polar angle, having an average value of around 11 % for the majority of physics processes that we study in *BABAR*. The dE/dx resolution from the SVT is typically about 16 %.

The *BABAR* ring-imaging Cherenkov detector (DIRC) provides dedicated charged particle identification in the central part of the detector. The polar angle coverage in the laboratory frame is $-0.84 < \cos\theta < 0.90$. The Cherenkov angle resolution of the DIRC is measured to be 2.4 mrad, for the quartz refractive index of 1.473, which provides better than $3\,\sigma$ separation between charged kaons and pions over a broad kinematic range.

The *BABAR* electromagnetic calorimeter (EMC) consists of an array of 6580 CsI(Tl) crystals, which encloses the tracking system and DIRC. The crystals have a truncated trapezoidal shape, and are finely segmented in the plane transverse to particles coming from the nominal e^+e^- interaction point (IP), with a typical cross-section of $4.7 \times 4.7\,\mathrm{cm}^2$ at the front and $6.0 \times 6.0\,\mathrm{cm}^2$ at the back. The crystals range in depth between 16 and 17.5 radiation lengths (the radiation length of CsI(Tl) is 1.85 cm), with the crystal axis pointing back roughly to the IP. The EMC geometry can be approximately described as a central cylindrical barrel, divided into forward ($26.93^\circ < \theta \leq 90^\circ$) and backward ($90^\circ < \theta \leq 140.81^\circ$) regions, plus a conical forward endcap ($15.76^\circ < \theta \leq 26.81^\circ$). The crystals are staggered so that their front face presents a nearly normal surface to particles coming from the IP. The EMC covers about 90 % of the polar angle and all of the azimuth in the center-of-mass system of the collisions produced in PEP-II (see Fig. 1).

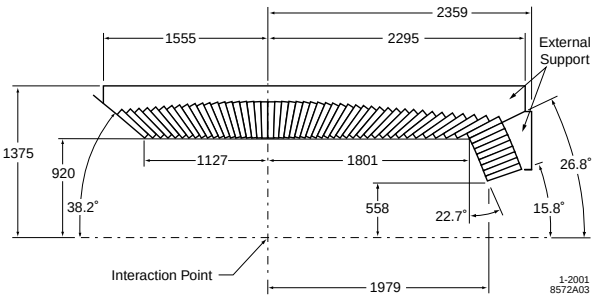

Fig. 1. Longitudinal cross section of the EMC showing the top half of the detector. All dimensions are given in mm.

The energy resolution of the calorimeter has been measured *in-situ* using a combination of radioactive sources, symmetric decays of π^0 and η, and Bhabha events, and can be described as:

$$\frac{\sigma_E}{E} = \frac{(2.30 \pm 0.30)\%}{\sqrt[4]{E(\mathrm{GeV})}} \oplus (1.35 \pm 0.22)\%, \qquad (2)$$

where E and σ_E refer to the shower energy and its rms error, measured in GeV. The angular resolution is limited by the transverse crystal size and the distance from the IP. It can also be parameterized as an energy-dependent function

$$\sigma_\theta = \sigma_\phi = \frac{(4.16 \pm 0.04)}{\sqrt{E(\mathrm{GeV})}}\,\mathrm{mrad}. \qquad (3)$$

The EMC is surrounded by a series of 108 iron plates arranged as coaxial octagonal cylinders about the *BABAR* symmetry axis. These plates form a high-susceptibility path for the magnetic flux generated by the *BABAR* solenoid to close on itself. Between the

iron plates are resistive plate chambers and limited streamer tubes with binary readout, used to track muons and provide crude neutral hadron detection. The innermost layers of muon chambers act effectively as a 'tail catcher' for the EMC, detecting particles from showers that leak out the back.

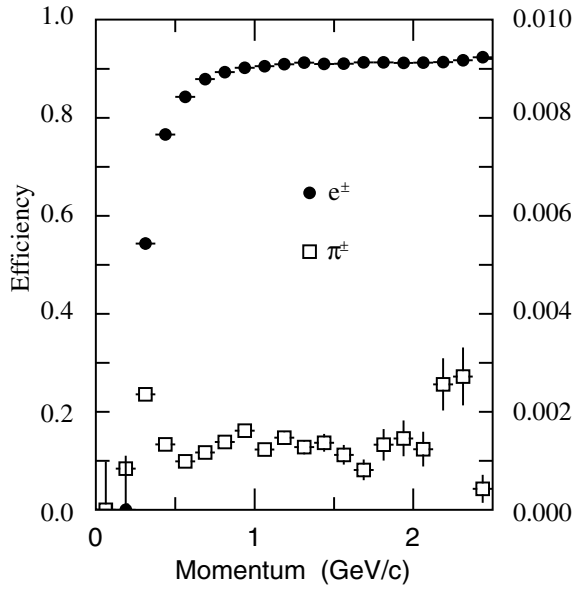

Fig. 2. Electron efficiency and pion misidentification probability as a function of the particle momentum, measured in the laboratory system. Note the different scales for electrons (left) and pions (right).

Electron-pion discrimination at *BABAR* is accomplished primarily by comparing the deposited shower energy with the track momentum, by modeling the lateral shower profile, and by looking for shower leakage in the muon chambers following the EMC. Figure 2 shows the electron efficiency and pion misidentification probability as a function of the particle momentum, using the standard *BABAR* electron selection algorithm [5]. This algorithm combines the above information into a likelihood ratio, using parameterized probability density functions (PDFs) fit to data control samples. The average electron identification efficiency is found to be 92 %, while the pion misidentification probability varies between 0.04 % and 0.28 %. A substantial degradation of the electron-pion separation, particularly of the electron efficiency, occurs for momentum below 500 MeV/c, due to the increase of the charge-exchange cross section (where charged pions convert to π^0) and reduced shower leakage. Information about the longitudinal shower development would reduce the pion misidentification from both these causes in this momentum region.

3. Longitudinal Shower Depth Variable

To derive longitudinal shower development information from *BABAR* we exploit the fact that most particles do not enter the calorimeter exactly parallel to the crystal axes. A non-zero entrance angle transforms the transverse crystal segmentation into an effective longitudinal segmentation, providing some depth information. Because the effective longitudinal segmentation is poor (often fractional) and different for every particle, we do not attempt a full parameterization of the longitudinal shower development. Instead, we characterize the shower by the first moment of its longitudinal development, which we call the *Longitudinal Shower Depth* (ΔL). The ΔL value is closely related to, but not identical to, the position of the electromagnetic shower maximum, as is discussed in Appendix A.

The ΔL variable is a geometric quantity which exploits the fact that the track and the cluster both sample different two-dimensional projections of the three-dimensional shower spatial distribution. When the track direction is not parallel to the crystal axis, these projections are not fully degenerate, and they can be combined to extract the otherwise unobservable, third (longitudinal) dimension.

Three effects are responsible for the fact that the track direction and the crystal axes are not collinear. First, the magnetic field bends the track as it passes through the tracking volume. Second, the width of the beamspot in the beam direction causes tracks from the IP to have a different polar angle from that of the axis of the crystal they strike. Finally, by design, the crystal axes of the *BABAR* calorimeter do not project perfectly back to the nominal IP, which reduces the chance of particles from the IP passing perfectly between crystals.

As part of computing ΔL we describe the calorimeter cluster as a directed line segment in space. We first compute the two-dimensional cluster centroid using the standard *BABAR* algorithm, which takes the weighted average of the crystal center positions at a nominal depth of 12 cm, using a logarithm of the crystal energy as weight [6]. We then compute the weighted average direction of the crystal axes, using the energy in each crystal as (linear) weight. The cluster line segment is defined to pass through the cluster centroid, and point in

the average crystal direction. The starting point of the cluster line segment is taken as the average position of the crystal front faces projected along the average direction.

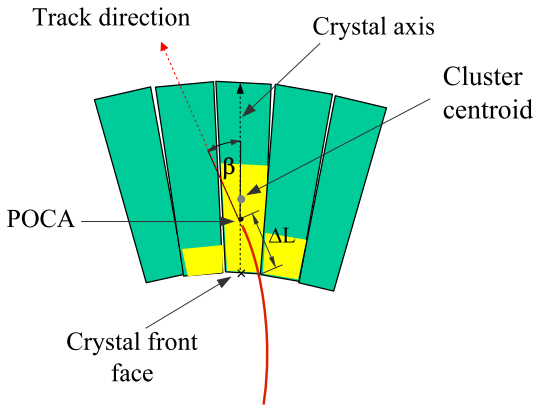

Fig. 3. Schematic view of how ΔL is calculated.

We then calculate the point of closest approach (POCA) in three dimensions between the extrapolated track trajectory and the cluster line segment, using an iterative algorithm. The POCA is the point where the track and cluster projections of the particle trajectory are most consistent.

Conceptually, we define ΔL as the path distance the track travels in the calorimeter's active material in reaching the POCA. In practice, we define ΔL as the distance along the cluster line segment of the POCA, divided by the cosine of the angle between the track direction and the cluster line segment direction, given algebraically as:

$$\Delta L \equiv \frac{(\vec{r}_{\rm POCA} - \vec{r}_{\rm Front}) \cdot \hat{r}_{\rm Cluster}}{\cos\beta} \qquad (4)$$

where $\vec{r}_{\rm POCA}$ is the position of the POCA, $\vec{r}_{\rm Front}$ is a point on the front face of the crystal, $\hat{r}_{\rm Cluster}$ is a unit vector in the direction of the cluster line segment, and β is the angle between the track direction and the cluster axis direction. This quantity approximates the active material path distance, but is much simpler to compute. Our definition of ΔL ignores the effects of track curvature and crystal-face staggering, which are negligible on the scale of the resolution we achieve on ΔL. The definition of ΔL is presented graphically in Fig. 3.

4. Electron ID Performance Evaluation

In order to evaluate the sensitivity of ΔL for electron identification, we apply a likelihood-based approach to the control samples of electrons and pions. Because ΔL is not a strong discriminant, we combine it with two other variables: the ratio of the shower energy deposited in the calorimeter and the momentum of the track associated with the shower (E/p) and the lateral shower moment:

$$LAT = \frac{\sum_{i=3}^{N} E_i r_i^2}{\sum_{i=3}^{N} E_i r_i^2 + E_1 r_0^2 + E_2 r_0^2}. \qquad (5)$$

Here N is the total number of crystals associated to a shower, E_i is the energy deposited in the i-th crystal such that $E_1 > E_2 > .. > E_N$, r_i the lateral distance between center of the shower and i-th crystal as defined earlier, and $r_0 = 5$ cm which is approximately the average distance between two crystals. Our approach intends to provide a more realistic evaluation taking into account possible correlations between the longitudinal variable and stronger discriminants.

The considered control samples comprise about one million electron and four million pion candidates selected from a reasonable dataset collected with the *BABAR* detector during the year 2005-2006. The data were collected at the PEP-II asymmetric energy e^+e^- collider (9 GeV e^- and 3.1 GeV e^+), resulting in a center-of-mass energy suitable for coherent $B\overline{B}$ production and subsequent decay at the $\Upsilon(4S)$ resonance. In the following two subsections, we briefly outline the salient features of these control samples.

4.1. *Electron Control Samples*

We select electrons [1] in both radiative and nonradiative Bhabha events ($e^+e^- \to e^+e^-(\gamma)$) by utilizing requirements on the energy deposit and shower-shape variables in the EMC, and by rejecting track candidates consistent with being muons. Based on Monte Carlo studies, the purity of this sample is found to be 99.9 %. As the Bhabha events provide mostly high momenta electrons, we consider the two-photon mediated process $e^+e^- \to (e^+e^-)\gamma^*\gamma^* \to (e^+e^-)e^+e^-$ to enhance statistics in the lower-to-medium momentum range ($p < 3$ GeV/c). The idea behind this sample selection is that the two initial

[1] Electrons denote both electrons and positrons.

state electrons tend to retain large longitudinal momenta and high energies, while the two-photon produced electrons have large transverse momenta and low energies. The selection requirement for this process provides a clean sample of electrons with purity comparable to that of the Bhabha events.

Figure 4 shows distributions of the ΔL variable *vs.* the track momentum for electrons selected in these two control samples.

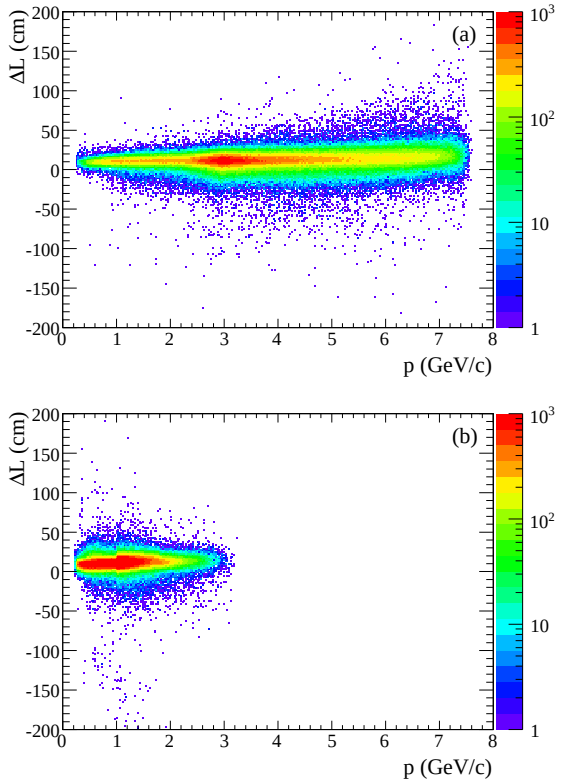

Fig. 4. Distributions of ΔL *vs.* track momentum of electrons selected in (a) Bhabha Sample and (b) two-photon mediated process. The color (intensity) scale is arbitrary.

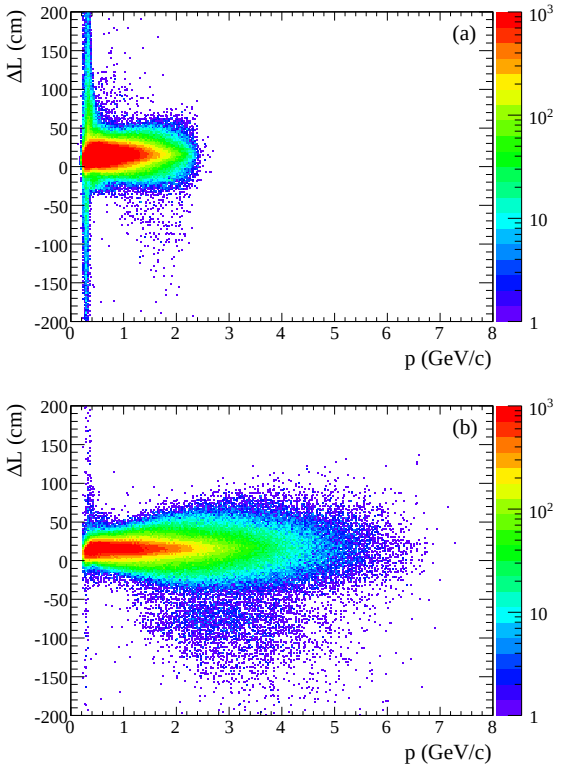

Fig. 5. Distributions of ΔL *vs.* track momentum for pions selected in (a) $K^0_S \to \pi^+\pi^-$ and (b) $e^+e^- \to \tau^+\tau^-$ events. The color (intensity) scale is arbitrary.

4.2. *Pion Control Samples*

The K^0_S lifetime is sufficiently long to produce a decay vertex that is well separated from the IP. Hence the process $K^0_S \to \pi^+\pi^-$ is easy to identify, yielding a pure pion sample. The purity of this sample selection, determined with a mixture of simulated $B\overline{B}$ decays and $e^+e^- \to q\overline{q}$ continuum events, is found to be $\sim$ 99.5 %. Although the K^0_S pion sample is very clean, it does not provide many pions at momenta above 1.8 GeV/c. High momentum pions are selected from $e^+e^- \to \tau^+\tau^-$ events with 3-1 track topology. Monte Carlo studies indicate that this sample is more affected by contamination compared to the $K^0_S \to \pi^+\pi^-$ events, having a purity of about 97 % in the momentum region of interest ($>$ 1.8 GeV/c), that arises almost entirely due to kaons. However, this poses a little challenge for our study of electron-pion separation since the electron contamination in the τ-pair pion sample is exceedingly small.

Distributions of the ΔL variable as functions of the track momentum for both K^0_S sample pions and τ-pair pions are given in Fig. 5. The broad spread of ΔL values for tracks with momentum below 400 MeV/c comes from the large uncertainty in $1/\cos\beta$ for tracks which, due to magnetic bending, enter the EMC nearly perpendicular to the cluster direction (see Eq. (4) and Fig. 3). The small population of negative ΔL outliers at large momentum come from effects like particle shower overlap that can distort the cluster position enough to drive the POCA calculation to select the IP instead of the true track-shower consistency point.

5. Electron ID Results

To evaluate the significance of ΔL as a component of electron identification, we compare the performance of a likelihood-based electron identification algorithm with and without the use of ΔL. The performance is described in terms of the electron efficiency and pion rejection of the algorithm, measured in the electron and pion control samples discussed previously. We use the TMVA (Toolkit for Parallel Multivariate Data Analysis) package [7] to build a global likelihood function using the two strong discriminants E/p and LAT, together (or not) with ΔL.

To study the pion misidentification rate for a given value of electron ID efficiency, first we define a likelihood ratio, R_L, for each track candidate in the considered signal and background samples by:

$$R_L = \frac{L_S}{L_S + L_B}. \quad (6)$$

Here, the signal and background likelihoods (L_S, L_B) are products of corresponding probability density functions (p_S, p_B) of the three discriminating variables:

$$L_S(i) = \prod_{j=1}^{3} p_{S,j}(i). \quad (7)$$

After that, for a given value of the likelihood ratio, the signal efficiency and background rejection factor (the rejection is equal to 1− efficiency) are calculated. This is done for different momentum bins, separately in the forward and the backward barrel, and the endcap regions.

Figure 6 shows the electron efficiency *vs.* pion rejection factor for a typical low momentum bin ($0.2 < p \leq 0.4\,\mathrm{GeV}/c$) in the forward barrel EMC. It is evident that for any given value of electron identification efficiency the likelihood function based on ΔL gives a higher pion rejection factor, or conversely a lower misidentification probability compared to the case where ΔL is not included. Table 1 summarizes results obtained across the full kinematic range for various parts of the EMC. There is a clear improvement in the performance for the backward and forward barrel regions, while for the endcap region (where high momenta particles are mostly abundant), we find a marginal improvement. This is because the discrimination power of ΔL diminishes with energy.

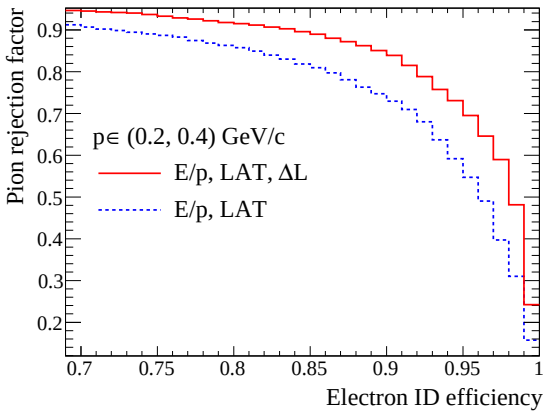

Fig. 6. Pion rejection factor as a function of electron identification efficiency in the forward Barrel region for a typical low momentum bin: $0.2 < p \leq 0.4\,\mathrm{GeV}/c$.

Table 1
Comparison of pion rejection factors at 95 % electron identification efficiency in the case where the likelihood function is defined with (without) ΔL.

p in	Backward Barrel		Forward Barrel		Endcap	
GeV/c	with	without	with	without	with	without
[0.2, 0.4]	55 %	46 %	70 %	55 %		
[0.4, 0.6]	61 %	53 %	73 %	61 %	87 %	85 %
[0.6, 0.8]	80 %	75 %	77 %	67 %		
[0.8, 1.0]	95 %	92 %	90 %	86 %		
[1.0, 2.0]	96 %	95 %	96 %	95 %	97 %	96 %
> 2.0	89 %	89 %	96 %	95 %		

6. Shower Depth in Particle ID

The ΔL variable can also be used to enhance general charged particle identification, as it is sensitive to the differing longitudinal shower development profiles of different particle species. This is demonstrated in Fig. 7, which plots ΔL for different species of particles, broken down into four track momentum bins, in simulated $B\overline{B}$ events. The histograms in these plots have been normalized to the same area, to better show the difference in the shape of the distributions.

At momenta below 400 MeV/c, all particle types lose energy primarily through ionization, and hence have similar longitudinal shower development. Additionally, the spatial resolutions of the tracking system and calorimeter are poor at these momenta, broadening the ΔL distribution. Because of both these effects, ΔL shows only weak particle discrim-

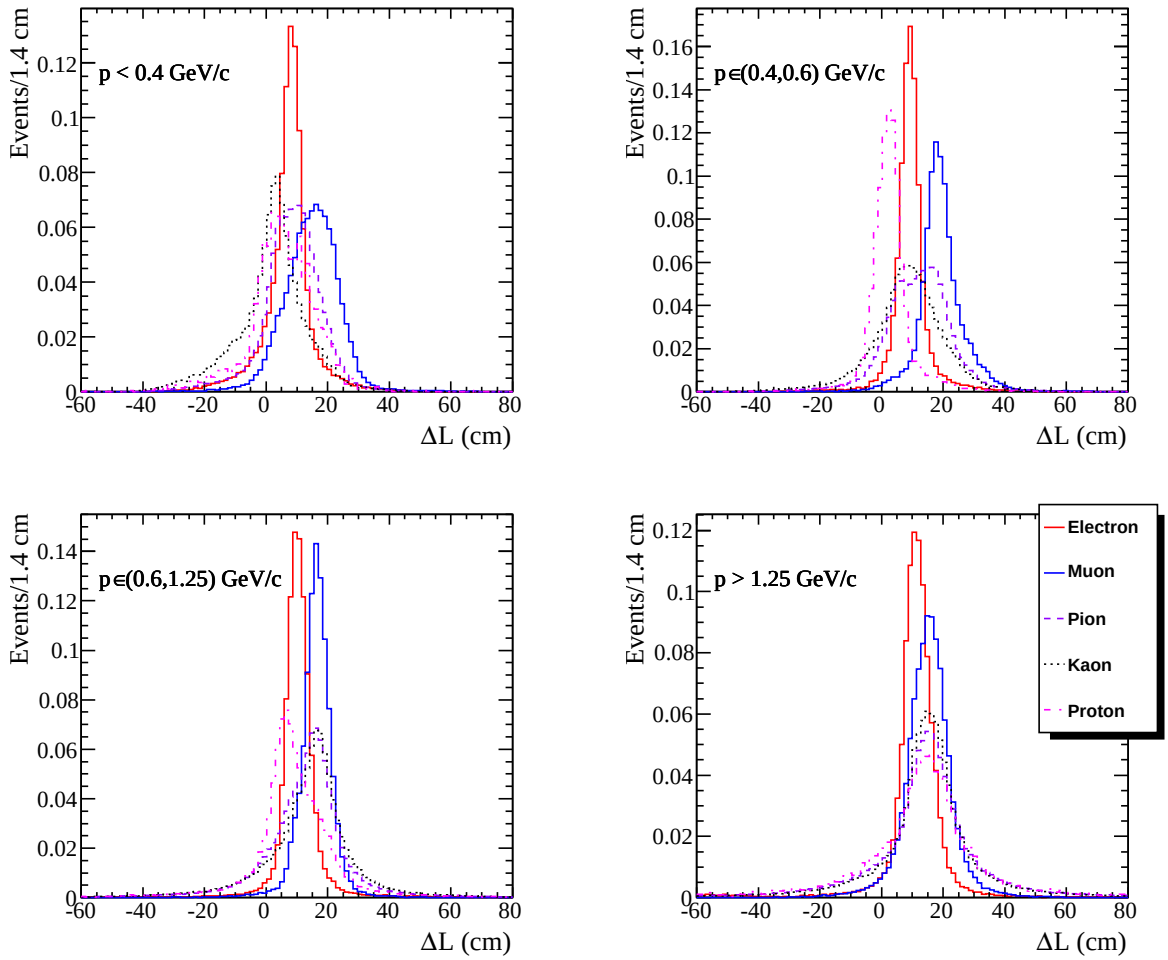

Fig. 7. Distributions of ΔL for different types of particles in different momentum bins from Monte Carlo $B\overline{B}$ events simulated in the *BABAR* detector. The histograms are normalized to unit area.

ination capability at very low momenta.

At momenta above 1.25 GeV/c, the decrease in magnetic bending reduces the separation between the track and crystal axes, degrading the particle separation power of ΔL. The greater width of the ΔL distribution for hadrons compared to leptons offers only a weak PID discrimination at high momentum compared to the DIRC in this region.

At intermediate momenta between 400 MeV/c and 1.25 GeV/c, ΔL shows a clear distinction between different particle species. Since protons are highly-ionizing and deposit most of their energy early in the crystal, their ΔL distribution peaks at small values. For electrons ΔL peaks near shower maximum ($\sim$ 10 cm). Because muons are minimum ionizing particles they distribute their energy uniformly along their path through the EMC, so ΔL for them peaks at roughly half the crystal length (20 cm). By contrast, the ΔL distributions from pions and kaons are broader, corresponding to the greater variability of hadronic showers. In this momentum region, ΔL offers approximately $0.8\,\sigma$ pion-muon separation [2], compared to about $1.5\,\sigma$ separation from the DIRC and less than $0.1\,\sigma$ separation from either DCH or SVT $\mathrm{d}E/\mathrm{d}x$ [9]. Thus ΔL provides a useful cross-check to the DIRC when identifying muons at intermediate momenta, and provides the best muon-pion separation for the 15 % of the *BABAR* solid angle covered by tracking and calorimetry but not by the DIRC.

[2] We define σ as the quadratic average of the pion and muon ΔL distribution rms *i.e.* $\sqrt{(\sigma_\mu^2+\sigma_\pi^2)/2}$.

7. Energy Evolution of Shower Depth

For electrons we expect the shower maximum position to evolve logarithmically with energy [8]. To the extent that ΔL is related to shower maximum, we might expect that to evolve logarithmically with energy as well.

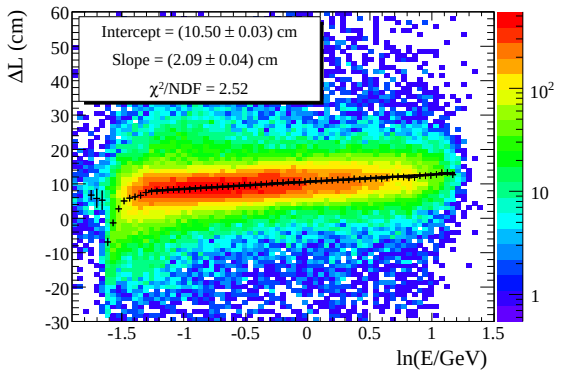

Fig. 8. Logarithmic dependence of ΔL on electron energy for true electrons in Monte Carlo $B\overline{B}$ events simulated in the *BABAR* detector.

Figure 8 shows ΔL for electrons against the natural log of the electron energy in simulated *BABAR* $B\overline{B}$ events, where one of the two B mesons is required to decay semileptonically to either a muon or an electron. The electron energy is estimated as the momentum of the track calculated at the point where the track enters the EMC after traversing the tracking volume. The data are sliced along the horizontal axis, each slice is fit to a Gaussian, and the Gaussian mean value (with its error) is plotted on top of the data. The data show a roughly linear dependence, demonstrating that ΔL behaves qualitatively similar to the shower maximum. The nonlinearity visible in the region below $\ln(E/\mathrm{GeV}) \approx -1.2$ *i.e.* $E < 300$ MeV comes from energy loss as the electrons pass at a large incidence angle through the quartz-bars of the DIRC, reducing the energy of the shower compared to the track momentum. The linear region of these data is fitted to a straight line, giving an intercept and slope of (10.50 ± 0.03) cm and (2.09 ± 0.04) cm, respectively (statistical errors only). These are close to the expected values of intercept and slope of 10.29 cm and 1.66 cm, respectively, as computed in Appendix A.

We have also examined the dependence of ΔL on electron energy in the *BABAR* data two-photon control sample described in Section 4. Figure 9 shows ΔL *vs.* the natural log of the electron energy in this control sample. The fitted intercept and slope are (11.36 ± 0.01) cm and (2.36 ± 0.03) cm, respectively (statistical errors only), again in reasonable agreement with the expected values of intercept and slope computed in Appendix A.

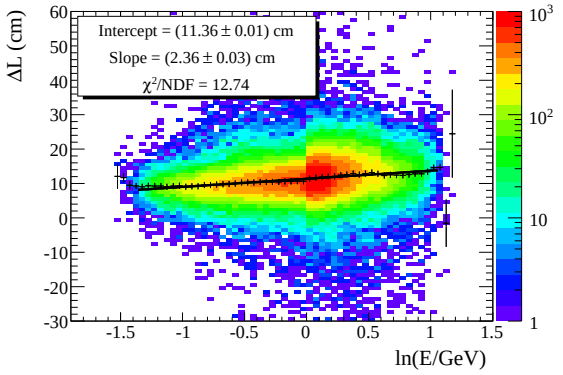

Fig. 9. Logarithmic dependence of ΔL on electron energy for electrons in the *BABAR* data two-photon control sample.

8. Conclusions

In this paper, we have presented a novel technique for extracting longitudinal shower development information from a crystal calorimeter in conjunction with a precision tracking system. When the derived quantity ΔL is used in electron identification, we have shown that the algorithm performance is significantly enhanced, especially in the low momentum region. We have also shown that ΔL has the potential to improve particle separation for other types of particles, particularly between muons and pions, in the low to intermediate momentum region. Finally, by studying the energy evolution of ΔL for electrons in *BABAR*, we have established that it behaves consistently with expectations from a standard longitudinal shower model computation.

9. Acknowledgments

The work presented in this paper could not have been accomplished without the help of many people. Many of the ideas were germinated and polished during our inspiring discussions with Helmut Marsiske. We also thank Paul Harrison, Chris Hawkes, Martin Kocian, Milind Purohit, and the members of the *BABAR* EMC and PID subgroups for their helpful comments and suggestions throughout this study; and *BABAR* and PEP-II for providing the data. The authors acknowledge the support from DOE and NSF (USA), and STFC (United Kingdom). Part of this work was supported by the Director, Office of Science, Office of High Energy Physics, of the U.S. Department of Energy under Contract No. DE-AC02-05CH11231.

Appendix A. Energy-weighted shower depth

The mean longitudinal profile of the energy deposition in an electromagnetic shower can be well described by a gamma distribution [8]:

$$\frac{dE}{dt} = E_0\, f(t) \;\text{ with } f(t) = \frac{1}{\Gamma(a)}\,(bt)^{a-1}\, b\, e^{-bt}, \quad \text{(A.1)}$$

where t is the distance measured in units of radiation length X_0, E_0 is the energy of the incident particle and E is the energy deposited by the particle at a certain distance t. Here $b \approx 0.5$ and $a = (1 + b\, t_{\max})$, where $t_{\max}$ denotes the shower maximum and is expressed as follows:

$$t_{\max} = \ln(E_0/E_c) + C_j, \;\; j = e, \gamma, \quad \text{(A.2)}$$

where $C_e = -0.5$ for electron-induced showers and $C_\gamma = +0.5$ for photon showers. To a good approximation, the critical energy E_c is given as $E_c = 0.8\,\text{GeV}/(Z + 1.2) = 0.0145\,\text{GeV}$ (for CsI(Tl), average $Z = 54$).

We can then solve for the energy-weighted longitudinal shower depth, ΔL, by integrating the fractional energy deposition per radiation length in Eq. (A.1), $f(t)$, with the corresponding path length t:

$$\Delta L \;= \int_0^L t\, f(t)\, dt = \frac{1}{\Gamma(a)} \int_0^L (bt)^a\, e^{-bt}\, dt \quad \text{(A.3)}$$

Here L indicates the average length of the CsI(Tl) crystal in units of X_0 and varies between 16 to 17.5 for various regions of barrel and endcap EMC. For simplicity, we took L to be 17.

As our goal is to deduce theoretically the intercept and slope of a linear function that we fit to the ΔL distribution *vs.* natural logarithm of the incident particles' energy, we decided to compute ΔL for two different values of $\ln(E_0/\text{GeV})$: 0 and 1. The first one is essentially the intercept, while their difference would give us the slope of the function. The above equation leads to:

$$\Delta L|_{\ln(E_0)=0} = \frac{1}{\Gamma(2.855)} \int_0^{17} (0.5t)^{2.855}\, e^{-0.5t}\, dt \quad \text{(A.4)}$$

and

$$\Delta L|_{\ln(E_0)=1} = \frac{1}{\Gamma(3.355)} \int_0^{17} (0.5t)^{3.355}\, e^{-0.5t}\, dt. \quad \text{(A.5)}$$

To derive the value of a, we substitute respective values of $t_{\max}$ to be 3.71 and 4.71 in the relation $a = 1 + b\, t_{\max}$. We compute the above two integrals as:

$$\Delta L|_{\ln(E_0)=0} = 5.562 \quad \text{(A.6)}$$

and

$$\Delta L|_{\ln(E_0)=1} = 6.425 \quad \text{(A.7)}$$

in units of X_0. We can translate Eqs. (A.6) and (A.7) by multiplying those with the radiation length of CsI(Tl) *i.e.* 1.86 cm which become 10.29 cm and 11.95 cm. From this we derive the intercept of the linear function fitted to ΔL *vs.* $\ln(E_0/\text{GeV})$ as 10.29 cm and the slope is 1.66 cm.

References

[1] ALICE Collaboration, "Technical Design Report of the Photon Spectrometer", CERN-LHCC-99-04; ATLAS Collaboration, "Liquid Argon Calorimeter", CERN-LHCC 96-41 and "Calorimeter Performance", CERN-LHCC-96-40; CMS Collaboration, "The Electromagnetic Calorimeter Technical Design Report", CERN-LHCC-97-33; and LHCb Collaboration, "LHCb Calorimeters : Technical Design Report", CERN-LHCC-2000-0036.

[2] Global Large Detector (GLD) Collaboration, arXiv:physics/0607154; Large Detector Concept (LDC), *http://www.ilcldc.org/documents/dod*; SiD Collaboration, *http://hep.uchicago.edu/∼oreglia/siddod.pdf*; and 4th Concept, *http://www.4thconcept.org/4doc.pdf*.

[3] L3 Collaboration, B. Adeva *et al.*, Nucl. Instrum. Meth. A 289 (1990) 35; CLEO-II Collaboration, Y. Kubota *et al.*, Nucl. Instrum. Meth. A 320 (1992) 66; KTeV

Collaboration, A. Alavi-Harati *et al.*, Phys. Rev. D 67 (2003) 012005, Erratum-ibid. D 70 (2004) 079904; and Crystal Ball Collaboration, S. Prakhov *et al.*, Phys. Rev. C 69 (2004) 045202.

[4] *BABAR* Collaboration, B. Aubert *et al.*, Nucl. Instrum. Meth. A 479 (2002) 1.

[5] T. Brandt, Chapter 4 of the thesis accessible from: *https://oraweb.slac.stanford.edu/pls/slacquery/BABAR_DOCUMENTS.DetailedIndex?P_BP_ID=3215*

[6] B.B. Brabson *et al.*, Nucl. Instrum. Meth. A 332 (1993) 419.

[7] TMVA Package, A. Höcker *et al.*, arXiv:physics/0703039.

[8] Particle Data Group, W.-M. Yao *et al.*, Section 27.5 of J. Phys. G 33 (2006) 1.

[9] Private communication with A.V. Telnov, Princeton University and the *BABAR* collaboration.